Geophysical Journal International

Geophys. J. Int. (2012) **189,** 1399–1408 doi: 10.1111/j.1365-246X.2012.05461.x

Magnetostratigraphy of the Xihe loess-soil sequence and implication for late Neogene deformation of the West Qinling Mountains

Junyi Ge,[1] Zhengtang Guo,[1] Tao Zhan,[1] Zhengquan Yao,[2] Chenglong Deng,[3] and Frank Oldfield[4]

[1]*Key Laboratory of Cenozoic Geology and Environment, Institute of Geology and Geophysics, Chinese Academy of Sciences, Beijing* 100029*, China. E-mail: ztguo@mail.iggcas.ac.cn*
[2]*Key Laboratory of Marine Sedimentology and Environmental Geology, First Institute of Oceanography, State Oceanic Administration, Qingdao* 266061*, China*
[3]*State Key Laboratory of Lithospheric Evolution, Institute of Geology and Geophysics, Chinese Academy of Sciences, Beijing* 100029*, China*
[4]*School of Environmental Sciences, University of Liverpool, Liverpool,* L69 7ZT*, UK*

Accepted 2012 March 15. Received 2012 March 13; in original form 2011 December 18

SUMMARY

The Qinling Mountain range forms an important climate barrier between southern and northern China. Its western part, referred to as the West Qinling, constitutes a unit of northeastern Tibetan Plateau. The uplift history of Qinling during the Neogene is still a contentious issue. Magnetostratigraphic results from the 150-m-thick Xihe loess-soil sequence (NL-VI), located on the alluvial highlands surrounding an intermontane basin from the West Qinling, indicate 17 reverse and 17 normal magnetozones. They are correlative with the interval from chron C5n to chron C2Ar in the Geomagnetic Polarity Timescale. The age of the NL-VI section can thus be palaeomagnetically constrained to a period from 10.5 to 4.2 Ma. The middle portion of the section has been affected intermittently by surface erosion processes. As loess is sensitive to any erosion that may have been induced by substratum deformation and tectonic uplift, this sequence indicates that the intermontane basin–ridge pattern of the West Qinling had already been formed by 10.5 Ma, thus providing suitable topographic conditions for aeolian deposition. This timing is consistent with a significant deformation phase between ∼14 and 10 Ma reported for the Tibetan Plateau. Meanwhile, the complete preservation of the NL-VI loess-soil sequence precludes both intense deformation of the substrate and rapid uplift of the West Qinling between 10.5 and 4.2 Ma. Although the erosion-affected portion of the NL-VI section reflects some degree of tectonic instability from 8.3 to 6.9 Ma, the intensity must have been sufficiently weak to prevent the erosion of the aeolian deposits. These further suggest that the late Miocene growth of the Tibetan Plateau has not significantly affected the West Qinling. Thus, the studied NL-VI aeolian sequence provides not only independent evidence for the uplift history of the West Qinling within an accurate chronological framework, but also provides new insights into the tectonic changes on the northeastern Tibetan Plateau.

Key words: Magnetostratigraphy; Rock and mineral magnetism; Tectonics and landscape evolution; Asia.

1 INTRODUCTION

Qinling (32°13.00′N–34°14.50′N and 104°13.00′E–112°14.50′E) is an east–west trending mountain range in central China extending for over 1500 km, with an average elevation of 2000–3000 m (Mattauer *et al.* 1985; Rost 1994). By forming a huge physical obstacle for the northward movement of the monsoon circulation, the range constitutes a critical climate boundary between northern and southern China with warm–humid subtropical climate in the south and cool–dry temperate climate in the north (Rost 1994; Yan 2006). Meng & Zhang (2000) suggested that the Qinling range experienced rapid uplift accompanied by strike-slip faulting in the Cenozoic, but the detailed deformation and uplift history histories within an accurate chronological framework remains unclear and has been attracted considerable attention. Some studies indicate that the Qinling range experienced episodic uplift from late Cretaceous times onwards, with major uplift probably occurred during the Palaeogene or/and Neogene (Wan *et al.* 2000; Yin *et al.* 2001) associated with the formation of the intermontane basins. There is also evidence suggesting significant uplift during the Pleistocene (Teng & Wang 1996; Xue *et al.* 2004).

The West Qinling Mountains, that is, the west part of the Qinling range, comprise part of the northeastern margin of the Tibetan Plateau (Fig. 1). It has been suggested that the lower crustal flow

from central Tibet diverted beneath the western Qinling and caused surface uplift, exhumation and deformation in this region to diminish eastward escape tectonics in the Cenozoic (Royden 1996; Enkelmann *et al.* 2006). Low temperature thermochronology reveals that early reverse faulting and associated mountain uplift in the West Qinling was initiated at ∼45–50 Ma in response to the growth of the Tibetan Plateau (Clark *et al.* 2005; Duvall *et al.* 2011). Deformation evidence for the early–late Neogene was also identified in recent years (e.g. Yu 1994; Enkelmann *et al.* 2006; Clark *et al.* 2010). For instance, volcanic activities in the Dangchang and Lixian regions took place episodically between 23 and 7 Ma (Yu 1994; Yu *et al.* 2006). The regions immediately north of the West Qinling show accelerated exhumation rates at ∼18–13 (Clark *et al.* 2010; Lease *et al.* 2011) and ∼9–4 Ma (Enkelmann *et al.* 2006). The West Qinling became a more pronounced source of sediment to the Linxia basin by ∼14 Ma (Garzione *et al.* 2005). Thus, the Neogene deformation history of the West Qinling is still ambiguous. An accurate chronological framework for this history needs to be reconstructed through various methods. In particular, the question as to when the ridge–intermontane pattern of the West Qinling was formed remains a critical issue to be solved.

Dating the sedimentary sequences within the intermontane basins in the Qinling Mountains could be expected to provide significant information for addressing this issue. In this regard, aeolian deposits are of particular value for tracing regional geomorphic or tectonic changes. This is based on two rationales: (1) the formation of loess requires a positive, relatively flat substrate topography that must be formed before the deposition of the overlying loess sequence and (2) loess is extremely sensitive to erosion, thus any significant tectonic/geomorphic change would cause extensive erosion. Accordingly, investigations on the distribution, chronology and completeness of the aeolian deposits from the various geomorphic units may be expected to provide reliable information relative to the changes in substrate topography and to tectonically induced deformation and associated erosion.

Recently, our investigations reveal widespread aeolian deposits mantling the piedmont highlands surrounding the intermontane basins within the West Qinling (Guo *et al.* 2010). The wind-blown origin of these deposits has been demonstrated by soil micromorphology, geochemistry and grain size studies (Ge & Guo 2010). This study aims at (1) dating a representative aeolian sequence (NL-VI) near Xihe in Gansu Province using magnetostratigraphy method, (2) exploring the tectonic implications of the sequence relative to the Neogene uplift history of the West Qinling Mountains and (3) discussing the potential links between this history and the formation of the Tibetan Plateau.

2 GEOLOGICAL SETTING

The West Qinling range separates the North China Block and Qilian orogens from the South China Block and Songpan-Ganzi terrane (Fig. 1) (Ratschbacher *et al.* 2003; Zhang *et al.* 2004). The West Qinling fault and the Kunlun fault systems form the northern and southern boundaries, respectively. Several strike-slip faults have developed within the West Qinling, such as the Lintan fault, Zhouqu-Mianlue fault and the Fengxian-Taibai fault (Fig. 1). Under the controls of such a tectonic framework, a series of intermontane basins were formed within the West Qinling separated by high standing ridges (Zhang *et al.* 2005; Wang *et al.* 2011).

The Xihe basin is one of the NEE-oriented intermontane basins in the West Qinling, and was interpreted as a strike-slip, pull-apart basin developed in the late Cenozoic (BGMRGP 1989; Zhang *et al.* 2005). The piedmont alluvial highlands of the basin are mantled by aeolian deposits whereas the central basin is mainly filled with reddish and grey-greenish mudstones of fluvio-lacustrine origin. The alluvial deposits forming the piedmont highlands overlie the limestone of Middle-Devonian age (BGMRGP 1989).

The NL-VI section (34°04′14″N, 105°22′40″E) is located on the alluvial highlands surrounding the Xihe basin (Fig. 1), and exposed along the flanks of an elongated gully with a top elevation of 1875 m. The section is 150 m thick and contains three parts. The upper (0–65.2 m) and lower (98.2–150.2 m) parts are typical loess-soil sequences with alternating soil and loess layers. The middle part (65.2–98.2 m) contains soil and loess layers, but also 31 levels consisting of a mixture of loess, soil and rock fragments (1–45%). The poorly sorted, angular rock fragments vary from 0.1 to 20 cm in diameter. They are mainly composed of schist, slate, granite, gneiss and limestone. These characteristics are quite similar to those of the deposits exposed on the slopes of the nearby alluvial highlands, suggesting that these rock fragments are derived from the alluvial deposits.

The sequence contains a total of 188 visually definable soils. Their weathering or argilic horizons (B or Bt) are reddish brown (5YR 4/8) or bright brown (7.5YR 5/8) in colour, silty–clay or clay in texture, with moderate to strong prismatic structure. They are underlain by nodular or petrocalcitic calcareous horizons. Loess layers are yellow-brown (7.5YR 6/4) to bright brown (7.5YR 5/6) with massive structures.

3 SAMPLING AND METHODS

In this study, a total of 715 block samples oriented by magnetic compass were collected at 20–25 cm intervals. In the laboratory, samples were cut into standard cubic specimens of 2-cm edge length for palaeomagnetic measurements. All specimens were thermally demagnetized using the MMTD80 Thermal Demagnetizer.[1] Remanence measurements were made with a 2G Enterprises Model 760-R three-axis cryogenic magnetometer[2] installed in a magnetically shielded space (<300 nT). First, 150 specimens at about 1-m intervals were selected and were subjected to stepwise thermal demagnetization up to 610 °C with 13 steps and 10–50 °C temperature increments. As most of specimens yield stable characteristic remanent magnetizations (ChRMs) above 250 °C, the other samples were demagnetized from 250 to 630 °C with 8–10 steps. All the experiments were performed in the Palaeomagnetism and Geochronology Laboratory of Institute of Geology and Geophysics, Chinese Academy of Sciences.

1502 samples at 10 cm intervals were taken for magnetic susceptibility measurements. They were dried in air and measured using a Bartington MS2 meter.[3] Low-frequency magnetic susceptibility (χ) was measured on all samples using the 0.47 kHz sensor. 802 samples were measured for high-frequency magnetic susceptibility at 4.7 kHz. Frequency-dependent magnetic susceptibility (χ_{fd}) was calculated for these 802 samples.

Various techniques were used to determine the magnetic mineralogy of representative samples from different depth on the NL-VI section. χ–T curves from room temperature to 700 °C were obtained under Argon atmosphere with a KLY-3 Kappa bridge with a CS-3 high-temperature furnace (Agico Ltd., Brno). Hysteresis

[1] Magnetic Measurements Ltd., Aughton, Lancashire, UK.
[2] 2G Enterprises, Sand City, CA, USA.
[3] Bartington Instruments Ltd., Witney, Oxon, UK.

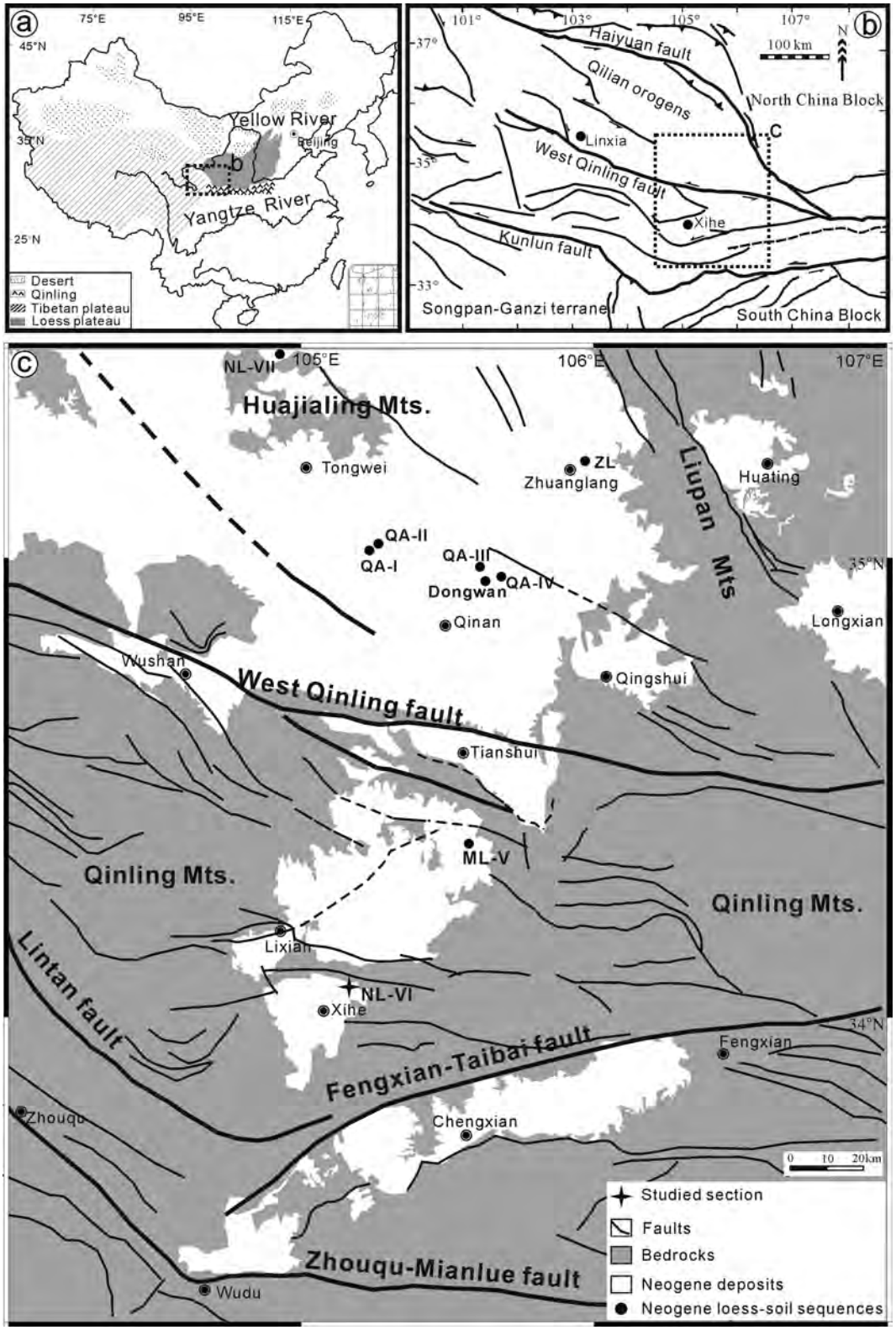

Figure 1. Location of the NL-VI section and the geological setting. (a) Location of the study area. The dotted rectangle outlines the area of Fig. 1(b); (b) geological setting of the NL-VI section [data for the faults are from Zhang *et al.* (2005) and BGMRGP (1989)]. The dotted rectangle outlines the area of Fig. 1(c); (c) map showing the location of the previously studied Neogene aeolian sequences with the detailed tectonic and geomorphologic settings.

loops for these samples were measured with a Princeton Micro-Mag 3900 Vibrating Sample Magnetometer[4] (VSM) in maximum magnetic field of 1.0 T. Saturation magnetization (M_s), saturation remanence (M_{rs}) and coercivity (B_c) were determined after correction for the paramagnetic contribution. Samples were then demagnetized in alternating fields (AF) up to 500 mT and isothermal

[4] Princeton Measurements Corporation, Princeton, NJ, USA.

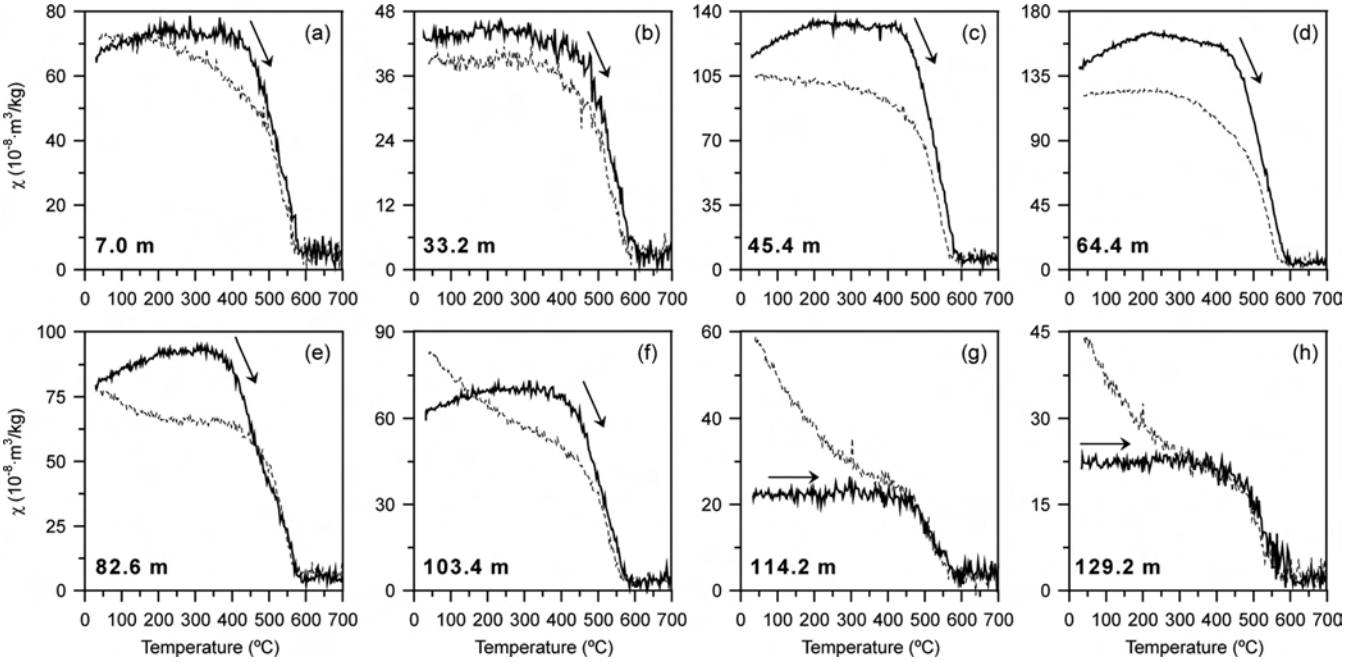

Figure 2. High-temperature magnetic susceptibility (χ–T) curves for typical samples from the NL-VI loess–palaeosol sequence. Solid (dotted) lines represent heating (cooling) curves.

remanent magnetizations (IRMs) were imparted from 0 to 1.0 T, using the MicroMag 3900 VSM. Subsequently, the saturation isothermal remanent magnetization (SIRM) (the IRM acquired at the maximum field of 1.0 T) was demagnetized in a stepwise direct current (dc) backfield to obtain the coercivity of remanence (B_{cr}).

4 RESULTS

4.1 Magnetic properties

The χ–T curves are characterized by a major decrease in magnetic susceptibility between 567 and 585 °C (Prévot *et al.* 1981, 1983; Fig. 2), the Curie point of magnetite, suggesting that magnetite is the main contributor to the susceptibility. A Curie point at 559–579 °C (Prévot *et al.* 1981, 1983) on the cooling curves indicates that the final product of the heating cycle is also magnetite. For most of the selected samples, the susceptibility along the cooling curve is close to or lower than the pre-heating values (Figs 2a–f). This behaviour points to a deficiency of weatherable Fe minerals in these loess/soil units, which if present, would serve as the source for the formation of new magnetite during laboratory heating (Deng *et al.* 2005). The susceptibility along the cooling curves for the older loess/soil units from the lower part of the NL-VI section show a gradual increase in susceptibility from about 400 °C to room temperature (Figs 2f–h), suggesting that a new magnetic material is produced by heating. This behaviour suggests a larger supply of weatherable Fe minerals in these older loess/soil units.

Most of the hysteresis loops are closed above 0.3 T (Figs 3a–f), which is consistent with the presence of a dominant ferrimagnetic phase. Some samples display wasp-waisted hysteresis loops, especially the samples from the lower section (Figs 3g and h). This arises from the coexistence of two magnetic components with strongly contrasting coercivities (Roberts *et al.* 1995), such as the combination of low-coercivity magnetite/maghaemite and high-coercivity haematite/goethite. Moreover, in light of underrepresentation owing to their weak magnetization, the wasp-waisted behaviour indicates a high concentration of hard, imperfect antiferromagnetic components (Roberts *et al.* 1995). Also, the hysteresis loops of all samples remain open up to 0.9 T, confirming significant contributions from high-coercivity phases. We interpret this behaviour as indicating the existence of haematite, despite the possibility that low-temperature oxidization of magnetite to maghaemite may contribute to the high coercivities (Van Velzen & Dekkers 1999; Liu *et al.* 2004).

The rapid rise of IRM below 0.1 T and the high values of S-ratio for most of the samples (Figs 4a–f) indicate the abundant presence of low-coercivity and ferrimagnetic minerals, such as magnetite and/or maghaemite. However, for some samples from the lower section (Figs 4g and h), the IRM continues to be acquired above 0.3 T, and the S-ratio exhibits lower values. These behaviours show a greater importance of a high-coercivity magnetic phase, such as haematite or goethite (*cf*. Hao *et al.* 2009).

4.2 Magnetic susceptibility and palaeomagnetic results

The χ values for the NL-VI sequence show clear variations corresponding to the field-defined lithological changes, with higher values in soils, as is a common feature for the Neogene loess-soil sequences in the western Chinese Loess Plateau (Guo *et al.* 2002, 2008; Hao & Guo 2004, 2007) and for the Quaternary loess-soil sequences (Liu & Ding 1998; Deng *et al.* 2005).

Demagnetization results were evaluated by orthogonal diagrams (Zijderveld 1967), and the principal component direction was computed by means of the principal component analysis (Kirschvink 1980) on a minimum of four consecutive steps, from the stable intermediate- and/or high-temperature components. For most samples, a secondary magnetic component, probably of viscous origin, was removed by thermal demagnetization at 250–300 °C, and the

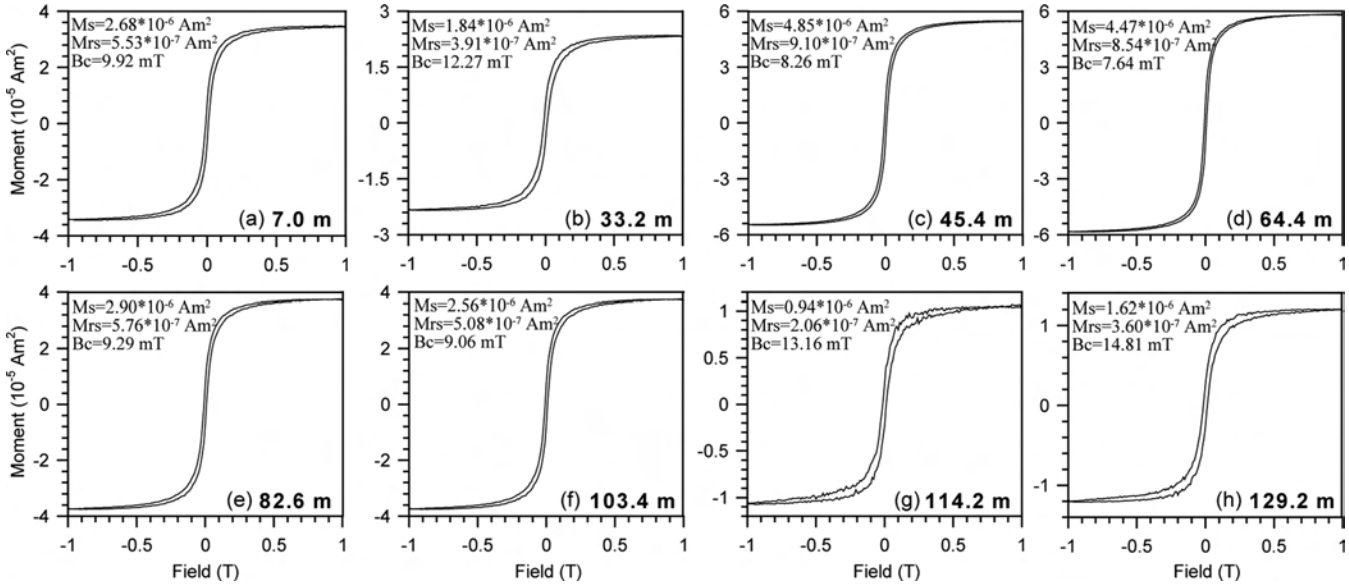

Figure 3. Hysteresis loops for representative samples after slope correction for paramagnetic contribution. These hysteresis loops were measured in fields up to ±1.0 T.

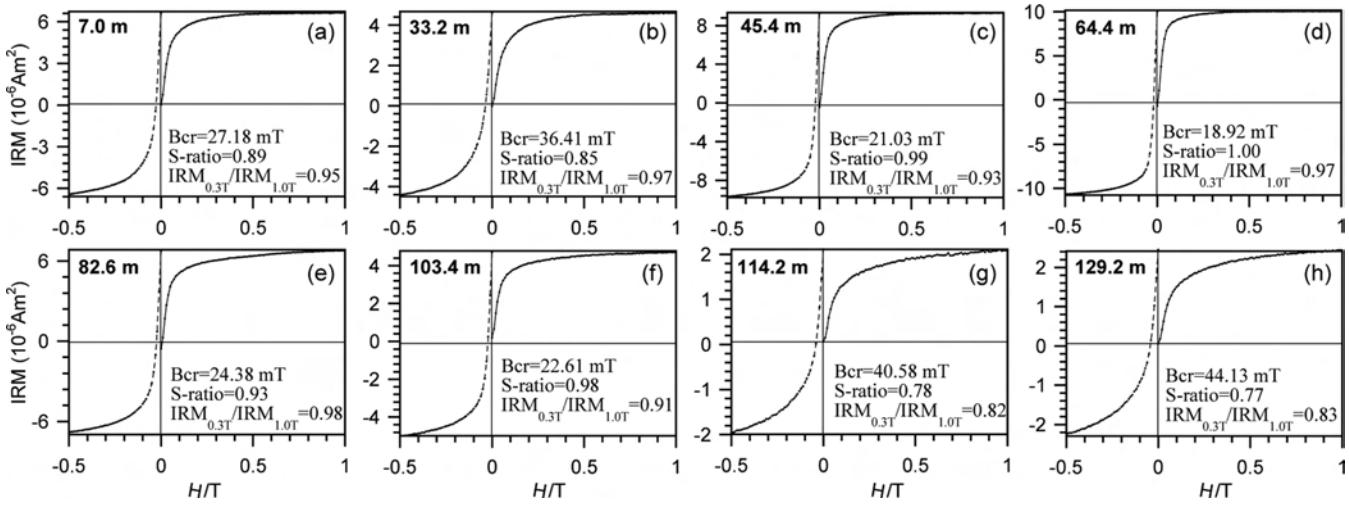

Figure 4. IRM acquisition curves and backfield curves of IRM for typical samples from the NL-VI section. The S-ratio, $(-\mathrm{IRM}_{-0.3\mathrm{T}})/(\mathrm{SIRM}_{1.0\mathrm{T}})$, is defined as the IRM remaining after exposure to a reversed field of 0.3 T divided by the SIRM (King & Channell 1991; Verosub & Roberts 1995).

high-stability ChRM component can be isolated between 300 and 585–610 °C (Fig. 5). These are consistent with the mineral magnetic results, indicating again that magnetite dominates the remanence carriers.

Among the 715 analysed samples, ∼51 samples were excluded owning to unstable demagnetization trajectories [for example, in case where it was not possible to isolate the ChRM directions, and/or where the ChRM directions gave a with maximum angular deviation (MAD) of >15°], or to ChRM directions giving Virtual Geomagnetic Pole (VGP) latitudes more than 45° from the mean VGP, which are regarded as outliers and transitional directions (Kirschvink 1980). Consequently, 664 samples yielded reliable ChRM directions, and the VGP latitudes were calculated from the ChRM data to construct the magnetostratigraphy of the NL-VI section (Fig. 6). Following demagnetization, 17 normal and 17 reverse magnetozones, defined by at least two successive levels of the same polarity, can be recognized in the sequence from the section (Fig. 6).

5 DISCUSSION

5.1 Correlation of the recognized polarity sequence to the GPTS

The magnetozones determined for the NL-VI section can be well correlated to the geomagnetic polarity timescale (GPTS; Gradstein *et al.* 2004). The interval from 0.6 to 43 m is correlative with the Gilbert reverse chron with the four normal magnetozones corresponding to the Cochiti, Nunivak, Sidufjall and Thvera normal subchrons, respectively (Fig. 6). The reverse magnetozone from 0 to 0.6 m can thus be definitely correlated to chron C2Ar within the Gilbert. The three normal magnetozones between 43 and 70.6 m are correlative with chrons C3An.1n, C3An.2n and C3Bn, respectively. The C3Br with two short normal polarity zones is identified between 70.6 and 79.6 m. The interval between 79.6 and 116.2 m contains two long normal and one long reverse magnetozones correlative with C4n.2n, C4An and C4r.2r, respectively. The portion between

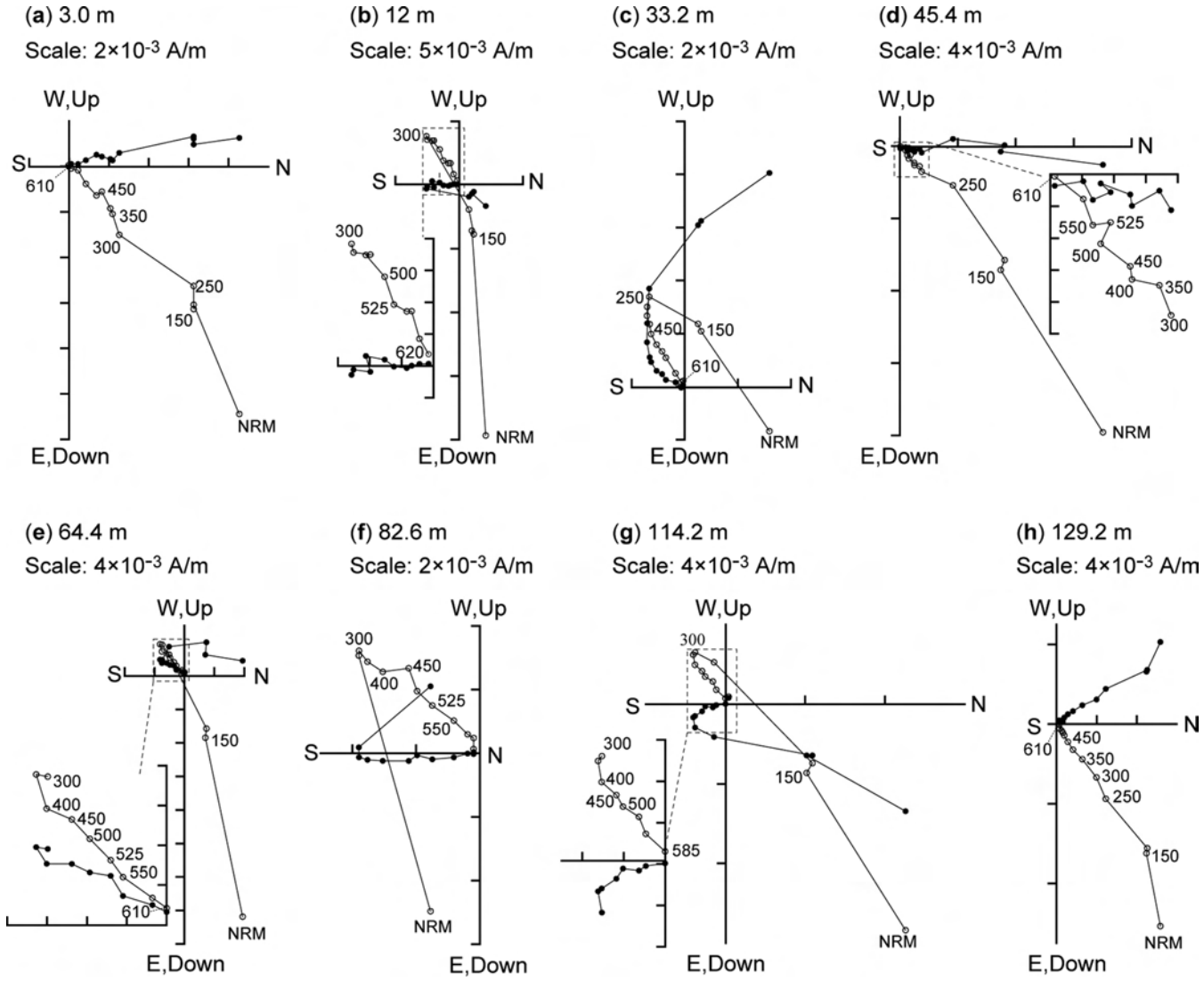

Figure 5. Orthogonal projections of representative progressive thermal demagnetization. The open (solid) circles refer to the vertical (horizontal) planes. The numbers refer to temperatures in °C. NRM, natural remanent magnetization.

116.2 and 135.75 m correlates well with C4Ar, with two normal and three reverse zones. The section ends within the thick normal polarity C5n (Fig. 3). Thus, the results define a nearly continuous sequence from chron C5n to chron C2Ar. The magnetostratigraphy of the NL-VL section indicates relatively stable sedimentation rates of ∼2.37 cm ka^{-1} from 10.5 to 4.2 Ma (Fig. 6). Extrapolations according to the average sediment accumulation rate yield a basal age of 10.49 Ma and a top age of 4.16 Ma for the section. The upper (65.2 m) and lower (98.2 m) boundaries of the gravel-bearing portion are dated to 6.93 and 8.30 Ma, respectively.

Magnetic susceptibility has proved to be useful for stratigraphic correlation of the late Miocene loess-soil sequences in the western Loess Plateau (Guo *et al.* 2002, 2008; Hao & Guo 2007; Liu *et al.* 2005; Zhan *et al.* 2010). Except for the gravel-bearing portion from 52.0 to 63.3 m in the Dongwan section, the magnetic susceptibility trends of the NL-VI section can be correlated with those of the Dongwan section (∼117 km north; Hao & Guo 2004; Figs 6b and e), confirming again that susceptibility of the Neogene loess-soil sequences can be used as a tool for stratigraphic correlation. The magnetochronology proposed is, thus, entirely consistent with the mammalian biochronology (Ge & Guo 2010) and with the broad correlation of susceptibility between the NL-VI and Dongwan sections.

5.2 Formation of the configuration of the ridge–intermontane basin system by 10.5 Ma

Formation of loess-soil sequences requires (1) drylands large enough to provide a significant amount of aeolian dust; (2) winds energetic enough for aeolian dust transport; (3) a fairly flat substrate topography for loess accumulation (Guo *et al.* 2008) and (4) a relatively stable tectonic environment to prevent the deposits from being eroded away.

Earlier studies demonstrated the onset of loess-soil formation in northern China by ∼22 Ma, indicative of seasonally alternative monsoon circulations and extensive deserts in the Asian inlands (Guo *et al.* 2002, 2008). In association with the previously reported Miocene aeolian sequences (Guo *et al.* 2002, 2008; Hao & Guo 2007; Liu *et al.* 2005; Zhan *et al.* 2010; Zhang *et al.* 2011; Fig. 1), the NL-VI section adds new insights about the widespread nature of the Miocene aeolian deposits, showing that the southern boundary

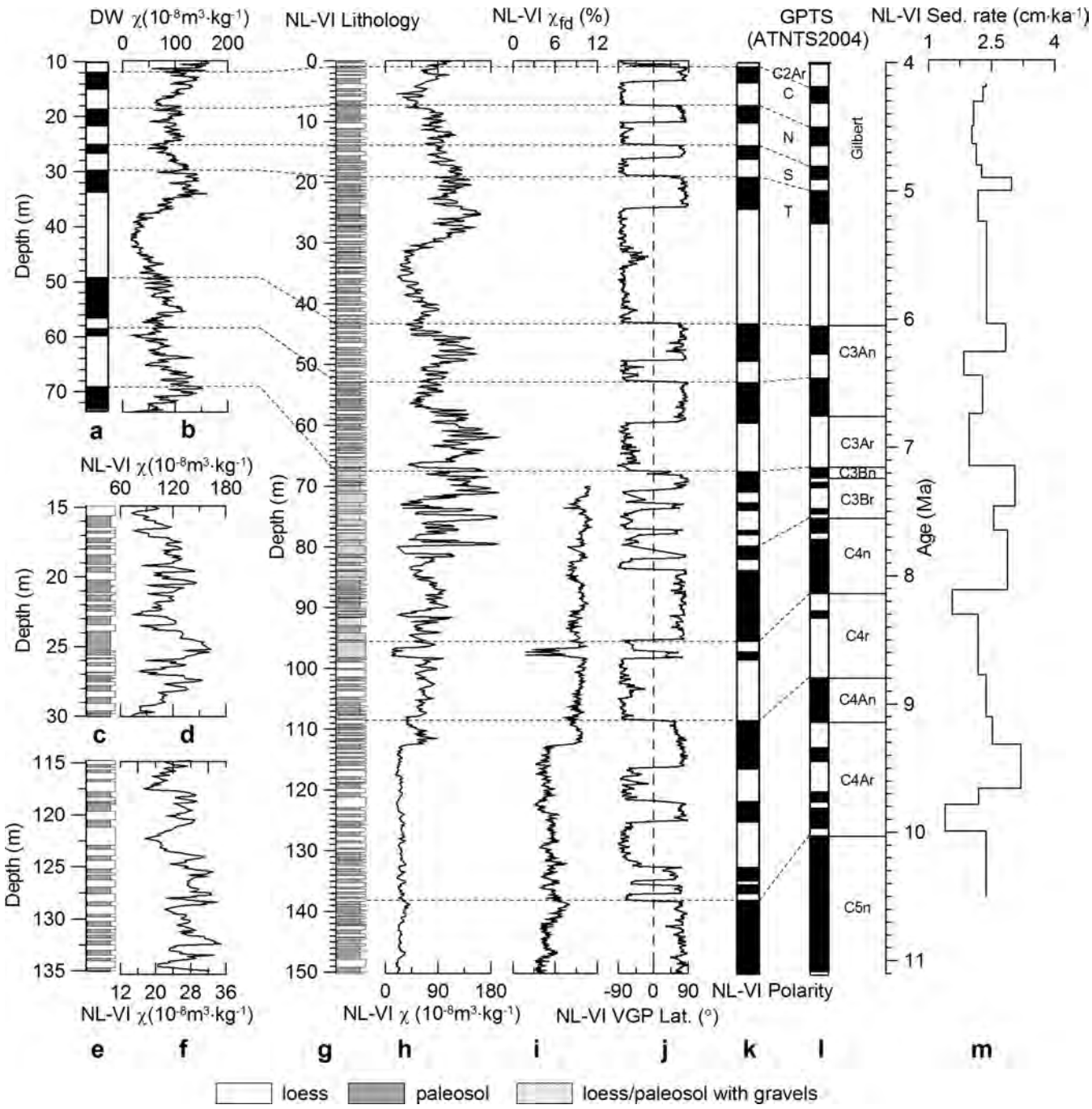

Figure 6. Magnetostratigraphy, magnetic susceptibility and sedimentation rate of NL-VI and correlations with the geomagnetic polarity timescale (GPTS). (a) Magnetic polarity of the Dongwan (DW) section (Hao & Guo 2004); (b) magnetic susceptibility of the Dongwan section (Hao & Guo 2004) and correlation with NL-VI; (c–d and e–f) zoomed lithology columns and magnetic susceptibility of NL-VI; (g) lithology of NL-VI; (h) magnetic susceptibility of NL-VI; (i) frequency dependent magnetic susceptibility of NL-VI; (j) VGP latitude of NL-VI; (k) magnetic polarity of NL-VI; (l) ATNTS2004 GPTS (Gradstein *et al.* 2004) and (m) sedimentation rate of NL-VI.

reached, at least, to ∼34°N. Its finer median grain size, averaging 6.1 μm (Ge & Guo 2010) compared to 7.5 μm at QA-I (∼120 km to the north) in the same time interval (6.2–10.5 Ma; Guo *et al.* 2002), confirms the northern location of the source region (the inland deserts) and the direction of the dust-carrying winds from the north by the Asian winter monsoon.

As loess is a kind of sediment extremely sensitive to erosion, the preservation of loess-soil sequences requires a relatively stable tectonic environment during and subsequent to their deposition. The NL-VI section is the first studied aeolian sequence of Miocene–Pliocene age from the Qinling Mountains. Its lithology and chronology provide independent information about the uplift history of the West Qinling range.

Intense aeolian deposition in the nearby region had already started by ∼22 Ma ago (Guo *et al.* 2002) whereas the lower boundary of the NL-VI aeolian sequence is dated to 10.5 Ma. This indicates that the substrate topography suitable for loess deposition near Xihe has already formed by ∼10.5 Ma. The onset of loess deposition near Xihe

is linked with tectonic, rather than climatic causes. A large-scale deformation would have occurred around this time and led to the formation of the stable alluvial highlands at least by ∼10.5 Ma. Since then, alluvial discharges mainly occurred via channels while the gentle slope (∼6–12°) of the alluvial highlands, generally covered by vegetation, preclude significant erosion by slope wash. These conditions provide a context in the mountains favourable to the receipt and continuous accumulation of aeolian dust.

Other studies indicate that a widespread deformation phase occurred widely in the West Qinling and adjacent regions during ∼14–10 Ma. $^{40}Ar/^{39}Ar$ dating for Cenozoic kamafugite from Dangchang-Lixian region indicates a significant strike-slip faulting episode initiated at ∼13 Ma (Yu 1994). This is temporally consistent with the transition from NNE–SSW compression to the WNW–ESE and/or E–W trending strike-slip along and to the south of the West Qinling fault (Wang *et al.* 2011). Rapid increases of sediment inputs from the West Qinling to the Linxia (Garzione *et al.* 2005) and Tianshui basins (Wang *et al.* 2007) by ∼14–10.8 Ma also support accelerated mountain exhumation. To the north of the West Qinling, the Jishi Shan (Lease *et al.* 2011), Helan Shan (Liu 2010) and some portion of the eastern Laji Shan (Lease *et al.* 2012) showed extensive exhumation due to strike-slip faulting during ∼13–10 Ma. Moreover, lithologic, magnetostratigraphic and stable isotope records from a number of small subbasins along the West Qinling fault, including Guide, Jian Zha, Xunhua, Tong Ren and Linxia, reveal that the basin segmentations leading to the separation of these basins was likely completed between ∼13 and 10 Ma (Hough *et al.* 2011), and steady lacustrine deposition in these basins would have initiated by 11–10 Ma. These observations support our conclusion that the stable ridge–intermontane basin systems had formed by at ∼10.5 Ma. A compilation of the major faults in the West Qinling, and their kinematic and dynamic characteristics, shows that significant strike-slip has been the dominant process responsible for this deformation phase (Enkelmann *et al.* 2006).

The Neogene deformation history of the West Qinling, as a part of the northeastern Tibetan Plateau, also provides valuable information concerning the tectonic history of the Tibetan Plateau. The formation of the ridge-basin system in the West Qinling by 10.5 Ma as defined by the NL-VI section and the significantly strike-slip faulting and exhumation that other studies documented (Garzione *et al.* 2005; Zhang *et al.* 2005; Hough *et al.* 2011) in this region and adjacent areas between ∼14 and 10 Ma are temporally consistent with some tectonic events reported from Tibet. These include at least the onset of E–W extension in the plateau interior at ∼14 Ma (e.g. Blisniuk *et al.* 2001), the expansion of the southeastern plateau margin after ∼13 Ma (e.g. Clark *et al.* 2005), and the development of new east-convergent thrust faults in northeastern Tibet by ∼13 Ma (Lease *et al.* 2011). These tend to suggest a plateau-wide deformation in the mid–late Miocene (Lease *et al.* 2011).

5.3 Tectonic instability between 6.9 and 8.3 Ma

The upper (6.9–4.2 Ma) and the lower (10.5–8.3 Ma) portions of the NL-VI section are typical loess-soil sequences. Their complete magnetozones define near continuous accumulation without any significant hiatus (Fig. 6). Our lateral correlation of the lithology showed that the complete preservation of loess sequences during these intervals is a common feature in the Xihe intermontane basin. This indicates a rather stable tectonic environment, as any significant tectonic activity would have caused loess erosion and led to discontinuities in the sequence.

The layers with mixed loess, soil and rock fragments in the middle section (65.2–98.2 m, from 8.30 to 6.93 Ma) indicate episodic surface erosions by water. The gravels were clearly derived from the alluvial deposits of the adjacent alluvial highlands. Although surface erosion may be induced by climatic changes, these episodic erosion features are unlikely to be attributable to climatic causes. First, the occurrences of these layers of mixed lithology are not preferentially linked to either loess or soil layers, indicating that erosion occurred within both cold–dry loess-forming or warm–humid soil-forming intervals. Second, the marine $\delta^{18}O$ record (Zachos *et al.* 2001) does not show any specific climatic event at this time despite of the overall global cooling trends during the late Cenozoic. Third, the weathering intensity of soil, as revealed by the frequency-dependent magnetic susceptibility (Fig. 6), does not exhibit any notable changes around the time when the first thick gravel layer from 98.2 to 94.5 m in depth occurred abruptly. This is also consistent with the insignificant soil colour changes observable in the field. We, therefore, interpret this gravel-bearing portion within NL-VI as evidence of tectonic instabilities.

This episode of tectonic instability and the consequent erosion has also been documented in other aeolian sequences on the Loess Plateau. For example, a water-reworked portion older than 6 Ma was reported from Dongwan (Hao & Guo 2004). In the eastern Loess Plateau, the lowermost portion of the Red Clay sequences at Xifeng (>6.2 Ma) and at Fugu (∼7 Ma) consists of a mixture of aeolian and colluvial sediments (Guo *et al.* 2001; Yue *et al.* 2007), indicating an erosion phase before 6.2 Ma. A loess erosion phase around the late Miocene was widely observed in the Tianshui-Qinan region, leading to the formation of shallow depressions filled with waterlain sediments (Yuan *et al.* 2007). Although a 11-Myr-old aeolian sequence in the eastern piedmont of the Luliang Mountains was recently reported (Xu *et al.* 2009), the lack of aeolian deposits older than 8 Ma in most of the eastern Loess Plateau indicates that the substrate topography east of the Liupan Mountains had developed by ∼8 Ma (Guo 2003; Hao & Guo 2004) suggesting fairly intense tectonic changes close to this time. These lines of evidence consistently define a tectonic event in the late Miocene in northern China. The gravel-bearing portion in the middle NL-VI section suggests that the event occurred between ∼8.3 and 6.9 Ma.

However, the relative completeness of the NL-VI section, as demonstrated by complete suite of magnetozones, precludes either significant folding deformation or intense uplift of the substrate in the West Qinling Mountains. At least, the event did not affect the basic pattern of the ridge–intermontane basins. Otherwise, the loess deposits would have been intensely eroded.

A wide range of observational evidence from the northeastern and eastern margins indicates that the Tibetan Plateau may have experienced major uplift around the late Miocene (Harrison *et al.* 1992; Métivier *et al.* 1998; Molnar 2005). It has also been suggested that the deformation front may have jumped ∼100 km outward to the Altyn and Liupan Shan at ∼8 Ma (Lease *et al.* 2011), leading to rapid exhumation of the Liupan Shan (Zheng *et al.* 2006) and Altyn Shan (Wan *et al.* 2001). The formation of the substrate topography for aeolian accumulation in the eastern Chinese Loess Plateau would also have occurred by ∼8 Ma (Guo 2003; Hao & Guo 2004). However, the relatively mild nature of the change in sedimentation, without obvious major unconformity in the NL-VI section from 8.3 to 6.9 Ma in the West Qinling Mountains would suggest that this late Miocene tectonic activity exercised a rather

weak influence to the West Qinling. The episodic instability (even probably earthquake events), as showed by the episodes of disturbed deposition and mixed lithology in the middle of the NL-VI section, might be a response to tectonic changes in distant regions.

6 CONCLUSIONS

The studied NL-VI section represents the first Neogene loess-soil sequence recovered from the southern slope of the Qinling Mountains. Our detailed palaeomagnetic measurements yield a complete set of magnetozones from chron C5n to chron C2Ar, and thus date the section for the period from 10.5 to 4.2 Ma. In association with the previously reported Miocene aeolian sequences from the Qinan region (Guo *et al.* 2002; Liu *et al.* 2005; Hao & Guo 2007), the top of the Huajialing Mountains (Zhan *et al.* 2010), from the terraces on the northeastern margin of the Tibetan Plateau (Lu *et al.* 2004) and near the Junggar Basin (Sun *et al.* 2010), it adds new insights about the widespread nature of aeolian deposition in northern China during the Miocene, with the southern boundary reaching at least to ∼34°N. These new data are in direct conflict with the earlier suggestion that aeolian deposition in northern China might have only been intensified at ∼8 Ma (Fan *et al.* 2006).

Because loess is a kind of sediment extremely sensitive to erosion, the NL-VI section provides an independent constraint upon the tectonic history of the West Qingling Mountains. It attests to the formation of the stable pre-loess topography, that is, the ridges–basin configuration pattern in West Qinling, by 10.5 Ma. The presence of well-preserved loess-soil sequence in West Qinling indicates that regional tectonic activities since 10.5 Ma were sufficiently gentle to prevent the loess deposits from being completely eroded away. This precludes significant folding deformation of the substratum or rapid/large amplitude uplift (mountain erosion) since the late Miocene.

We ascribe the signs of periodic, slight slope-water erosions in the middle section to episodic tectonic instability. This is consistent with the suggested tectonic changes for the Tibetan Plateau around the late Miocene (e.g. Molnar *et al.* 2010). The NL-VI section constrains the chronology of this regional tectonic instability in West Qinling ranging from 8.3 to 6.9 Ma, whereas the completeness of the upper and lower NL-VI section suggests rather stable tectonic environments at least between 10.5 (the basal age of the section) and 8.3 Ma and between 6.9 and 4.2 Ma (the top age of the section).

ACKNOWLEDGMENTS

This study was supported by the National Natural Science Foundation of China (Grants 40730104, 41002125) and the National Basic Research Program of China (Project 2010CB950200). We thank Q.Z. Hao and C.X. Zhang for helpful discussions, L. Liu and Y.Y. Yu for field and laboratory assistance, the editor and two anonymous reviewers for constructive comments and suggestions.

REFERENCES

BGMRGP, 1989. *Regional Geology of Gansu Province,* Geological Publishing House, Beijing.

Blisniuk, P.M., Hacker, B.R., Glodny, J., Ratschbacher, L., Bik, S., Wull, Z., McWilliams, M.O. & Calvert, A., 2001. Normal faulting in central Tibet since at least 13.5 Myr ago, *Nature,* **412,** 628–632.

Clark, M.K., House, M.A., Royden, L.H., Whipple, K.X., Burchfiel, B.C., Zhang, X. & Tang, W., 2005. Late Cenozoic uplift of southeastern Tibet, *Geology,* **33,** 525–528.

Clark, M.K., Farley, K.A., Zheng, D.W., Wang, Z.C. & Duvall, A.R., 2010. Early Cenozoic faulting of the northern Tibetan Plateau margin from apatite (U-Th)/He ages, *Earth planet. Sci. Lett.,* **296,** 78–88.

Deng, C.L., Vidic, N.J., Verosub, K.L., Singer, M.J., Liu, Q.S., Shaw, J. & Zhu, R.X., 2005. Mineral magnetic variation of the Jiaodao Chinese loess/paleosol sequence and its bearing on long-term climatic variability, *J. geophys. Res.,* **110,** B03103, doi:10.1029/2004JB003451.

Duvall, A.R., Clark, M.K., van der Pluijm, B.A. & Li, C., 2011. Direct dating of Eocene reverse faulting in northeastern Tibet using Ar-dating of fault clays and low-temperature thermochronometry, *Earth planet. Sci. Lett.,* **304,** 520–526.

Enkelmann, E. *et al.,* 2006. Cenozoic exhumation and deformation of northeastern Tibet and the Qinling: is Tibetan lower crustal flow diverging around the Sichuan Basin?, *Geol. Soc. Am. Bull.,* **118,** 651–671.

Fan, M.J., Song, C.H., Dettman, D.L., Fang, X.M. & Xu, X.H., 2006. Intensification of the Asian winter monsoon after 7.4 Ma: grain-size evidence from the Linxia Basin, northeastern Tibetan Plateau, 13.1 Ma to 4.3 Ma, *Earth planet. Sci. Lett.,* **248,** 186–197.

Garzione, C.N., Ikari, M.J. & Basu, A.R., 2005. Source of Oligocene to Pliocene sedimentary rocks in the Linxia basin in northeastern Tibet from Nd isotopes: implications for tectonic forcing of climate, *Geol. Soc. Am. Bull.,* **117,** 1156–1166.

Ge, J.Y. & Guo, Z.T., 2010. Neogene eolian deposits within the West Qinling Mountains: climate and tectonic implications, *Chinese Sci. Bull.,* **55,** 1483–1487.

Gradstein, F.M., Ogg, J.G. & Smith, A.G., 2004. *A Geologic Time Scale 2004,* Cambridge University Press, Cambridge.

Guo, Z.T., 2003. Uplifting of Tibetan Plateau and the eolian deposits in China, in *The Formation and the Environmental Development on the Tibetan Plateau,* pp. 70–79, ed. Zheng, D., Hebei Science Press, Hebei.

Guo, Z.T., Peng, S.Z., Hao, Q.Z., Biscaye, P.E. & Liu, T.S., 2001. Origin of the Miocene-Pliocene red-Earth formation at Xifeng in Northern China and implications for paleoenvironments, *Palaeogeogr. Palaeoclimatol. Palaeoecol.,* **170,** 11–26.

Guo, Z.T. *et al.,* 2002. Onset of Asian desertification by 22 Myr ago inferred from loess deposits in China, *Nature,* **416,** 159–163.

Guo, Z.T. *et al.,* 2008. A major reorganization of Asian climate by the early Miocene, *Clim. Past.,* **4,** 153–174.

Guo, Z.T. *et al.,* 2010. Comment on "Mudflat/distal fan and shallow lake sedimentation (upper Vallesian-Turolian) in the Tianshui Basin, Central China: evidence against the late Miocene eolian loess" by A.M. Alonso-Zarza, Z. Zhao, C.H. Song, J.J. Li, J. Zhang, A. Martín-Pérez, R. Martín-García, X.X. Wang, Y. Zhang and M.H. Zhang [Sedimentary Geology 222 (2009) 42–51], *Sediment. Geol.,* **230,** 86–89.

Hao, Q.Z. & Guo, Z.T., 2004. Magnetostratigraphy of a late Miocene-Pliocene loess-soil sequence in the western Loess Plateau in China, *Geophys. Res. Lett.,* **31,** L09209, doi:10.1029/2003GL019392.

Hao, Q.Z. & Guo, Z.T., 2007. Magnetostratigraphy of an early-middle Miocene loess-soil sequence in the western Loess Plateau of China, *Geophys. Res. Lett.,* **34,** L18305, doi:10.1029/2007GL031162.

Hao, Q.Z., Oldfield, F., Bloemendal, J., Torrent, J. & Guo, Z.T., 2009. The record of changing hematite and goethite accumulation over the past 22 Myr on the Chinese Loess Plateau from magnetic measurements and diffuse reflectance spectroscopy, *J. geophys. Res.,* **114,** B12101, doi:10.1029/2009JB00660.

Harrison, T.M., Copeland, P., Kidd, W.S.F. & Yin, A., 1992. Raising Tibet, *Science,* **255,** 1663–1670.

Hough, B.G., Garzione, C.N., Wang, Z.C., Lease, R.O. & Burbank, D.W., 2011. Stable isotope evidence for topographic growth and basin segmentation: implications for the evolution of the NE Tibetan Pleatau, *Geol. Soc. Am. Bull.,* **123,** 168–185.

King, J. & Channell, J., 1991. Sedimentary magnetism, environmental magnestism and magnestostratigraphy, *Rev. Geophys.,* **29,** 358–370.

Kirschvink, J.L., 1980. The least-squares line and plane and the analysis of palaeomagnetic data, *Geophys. J. astr. Soc.,* **62,** 699–718.

Lease, R.O., Burbank, D.W., Clark, M.K., Farley, K.A., Zheng, D.W. & Zhang, H.P., 2011. Middle Miocene reorganization of deformation along the northeastern Tibetan Plateau, *Geology,* **39,** 359–362.

Lease, R.O., Burbank, D.W., Hough, B.G., Wang, Z.C. & Yuan, D.Y., 2012. Pulsed Miocene range growth in northeastern Tibet: insights from Xunhua Basin magnetostratigraphy and provenance, *Geol. Soc. Am. Bull.,* doi:10.1130/B30524.1.

Liu, J.F., Guo, Z.T., Hao, Q.Z., Peng, S.Z., Qiao, Y.S., Sun, B. & Ge, J.Y., 2005. Magnetostratigraphy of the Miziwan Miocene eolian deposits in Qin'an County (Gansu Province), *Quat. Sci.,* **25,** 503–508.

Liu, J.H., 2010. Apatite fission track (AFT) analysis of the Cenozoic extensional exhumation and uplift of the Helan Shan and the Qinling mountains, and frictional heating along active faults, *Recent Dev. World Seism.,* **3,** 31–33.

Liu, Q.S., Banerjee, S.K., Jackson, M.J., Deng, C.L., Pan, Y.X. & Zhu, R.X., 2004. New insights into partial oxidation model of magnetites and thermal alteration of magnetic mineralogy of the Chinese loess in air, *Geophys. J. Int.,* **158,** 506–514.

Liu, T.S. & Ding, Z.L., 1998. Chinese loess and the paleomonsoon, *Ann. Rev. Earth. planet. Sci.,* **26,** 111–145.

Lu, H.Y. *et al.,* 2004. Geomorphologic evidence of phased uplift of the northeastern Qinghai-Tibet Plateau since 14 million years ago, *Sci. China Ser. D,* **47,** 822–833.

Mattauer, M., Matte, P., Malavieille, J., Tapponnier, P., Maluski, H., Qin, X.Z., Lun, L.Y. & Qin, T.Y., 1985. Tectonics of the Qinling belt: build-up and evolution of eastern Asia, *Nature,* **317,** 496–500.

Meng, Q.R. & Zhang, G.W., 2000. Geologic framework and tectonic evolution of the Qinling orogen, central China, *Tectonophysics,* **323,** 183–196.

Métivier, F., Gaudemer, Y., Tapponnier, P. & Meyer, B., 1998. Northeastward growth of the Tibet plateau deduced from balanced reconstruction of two depositional areas: the Qaidam and Hexi Corridor basins, China, *Tectonics,* **17,** 823–842.

Molnar, P., 2005. Mio-Pliocene growth of the Tibetan Plateau and evolution of Asian climate, *Palaeontol. Electron,* **8,** 1–23.

Molnar, P., Boos, W.R. & Battisti, D.S., 2010. Orographic controls on climate and paleoclimate of Asia: thermal and mechanical roles for the Tibetan Plateau, *Ann. Rev. Earth planet. Sci.,* **38,** 77–102.

Prévot, M., Lecaille, A. & Mankinen, E.A., 1981. Magnetic effects of maghemitization of oceanic crust, *J. geophys. Res.,* **86,** 4009–4020.

Prévot, M., Mankinen, E.A., Grommé, S. & Lecaille, A., 1983. High paleointensities of the geomagnetic field from thermomagnetic studies on rift valley pillow basalts from the mid-Atlantic ridge, *J. geophys. Res.,* **88,** 2316–2326.

Ratschbacher, L. *et al.,* 2003. Tectonics of the Qinling (Central China): tectonostratigraphy, geochronology, and deformation history, *Tectonophysics,* **366,** 1–53.

Roberts, A.P., Cui, Y. & Verosub, K.L., 1995. Wasp-waisted hysteresis loops: mineral magnetic characteristics and discrimination of components in mixed magnetic systems, *J. geophys. Res.,* **100,** 17 909–17 924.

Rost, K.T., 1994. Paleoclimatic field studies in and along the Qinling Shan (Central China), *GeoJournal,* **34,** 107–120.

Royden, L., 1996. Coupling and decoupling of crust and mantle in convergent orogens: implications for strain partitioning in the crust, *J. geophys. Res.,* **101,** 17 679–17 705.

Sun, J.M., Ye, J., Wu, W.Y., Ni, X.J., Bi, S.D., Zhang, Z.Q., Liu, W.M. & Meng, J., 2010. Late Oligocene–Miocene mid-latitude aridification and wind patterns in the Asian interior, *Geology,* **38,** 515–518.

Teng, Z.H. & Wang, X.H., 1996. Studies of the tectonic uplift at the Cenozoic era and the regionally environmental effects in the Qinling Orogenic Belt, *Geol. Shaanxi,* **14,** 33–42.

Van Velzen, A.J. & Dekkers, M.J., 1999. Low-temperature oxidation of magnetite in loess-paleosol sequences: a correction of rock magnetic parameters, *Stud. geophys. Geod.,* **43,** 357–375.

Verosub, K.L. & Roberts, A.P., 1995. Environmental magnetism: past, present, and future, *J. geophys. Res.,* **100,** 2175–2192.

Wan, J.L., Li, Q. & Wang, Y., 2000. The fission track evidence of Huashan Batholith uplifting in Mesozoic-Cenozoic, *Seism. Geol.,* **22,** 53–58.

Wan, J.L., Yu, W., Li, Q. & Wang, E.Q., 2001. FT evidence of Northern Altyn uplift in late-Cenozoic, *Bull. Mineral. Petrol. Geochem.,* **20,** 222–224.

Wang, X.X., Li, J.J., Song, C.H., Zhang, J., Zhao, Z.J., Gao, J.P. & Pan, M.H., 2007. Cenozoic uplift of West Qinling, northeast margin of Tibetan plateau—a detrital apatite fission track record from the Tianshui basin, *Earth Sci. Front.,* **1,** 304–308.

Wang, Z.C. *et al.,* 2011. Magnetostratigraphy and depositional history of the Miocene Wushan basin on the NE Tibetan plateau, China: implications for middle Miocene tectonics of the West Qinling fault zone, *J. Asian Earth Sci.,* **44,** 189–202, doi:10.1016/j.jseaes.2011.06.009.

Xu, Y., Yue, L.P., Li, J.X., Sun, L., Sun, B., Zhang, J.Y., Ma, J. & Wang, J.Q., 2009. An 11-Ma-old red clay sequence on the Eastern Chinese Loess Plateau, *Palaeogeogr. Palaeoclimatol., Palaeoecol.,* **284,** 383–391.

Xue, X.X., Li, H.H., Li, Y.X. & Liu, H.J., 2004. The new data of the uplifting of Qinling Mountains since the Middle Pleistocene, *Quat. Sci.,* **24,** 82–87.

Yan, J.P., 2006. *Comparable Studies on Environmental Changes in Southern and Northern Qinling Moutains,* China Science Press, Beijing.

Yin, G.M., Lu, Y.C., Zhang, H., Li, W.L., Li, L. & Guo, S.L., 2001. The tectonic uplift of the Hua Shan in the Cenozoic, *Chinese Sci. Bull.,* **46,** 1665–1668.

Yu, X.H., 1994. Cenozoic potassic alkaline ultrabasic volcanic rocks and its genesis in Lixian-Dangchang area, Gansu Province, *Tethyan Geol.,* **18,** 114–129.

Yu, X.H., Zhao, Z.D., Zhou, S., Mo, X.X., Zhu, D.Q. & Wang, Y.L., 2006. $^{40}Ar/^{39}Ar$ dating for Cenozoic kamafugite from western Qinling in Gansu Province, *Chinese Sci. Bull.,* **51,** 1621–1627.

Yuan, B.Y. *et al.,* 2007. Cenozoic evolution of geomorphic and sedimentary environments in the Tianshui-Qin'an regions, *Quat. Sci.,* **27,** 161–171.

Yue, L.P., Li, J.X., Zheng, G.Z. & Li, Z.P., 2007. Evolution of the Ordos Plateau and environmental effects, *Sci. China Ser. D,* **50,** 19–26.

Zachos, J., Pagani, M., Sloan, L., Thomas, E. & Billups, K., 2001. Trends, rhythms, and aberrations in global climate 65 Ma to present, *Science,* **292,** 686–693.

Zhan, T., Guo, Z.T., Wu, H.B., Ge, J.Y., Zhou, X., Wu, C.L. & Zeng, F.M., 2010. Thick Miocene eolian deposits on the Huajialing Mountains: the geomorphic evolution of the western Loess Plateau, *Sci. China Ser. D,* **54,** 1–8.

Zhang, G.W., Guo, A.L. & Yao, A.P., 2004. Western Qinling-Songpan continental tectonic node in China's continental tectonics, *Earth Sci. Front.,* **11,** 23–32.

Zhang, Y.Q., Ma, Y.S., Yang, N., Zhang, H.P. & Shi, W., 2005. Late Cenozoic left-slip faulting process of the east Kunlun-Qinling fault system in West Qinling region and its eastward propagation, *Acta Geosci. Sin.,* **26,** 1–18.

Zheng, D.W. *et al.,* 2006. Rapid exhumation at ∼8 Ma on the Liupan Shan thrust fault from apatite fission-track thermochronology: implications for growth of the northeastern Tibetan Plateau margin, *Earth planet. Sci. Lett.,* **248,** 198–208.

Zhang, Y., Xiong, S.F., Ding, Z.L., Lu, H.J. & Jiang, W.Y., 2011. Carbon-oxygen isotpe records of pedogenic carbonate from the Early Miocene-Pleistocene loess-Red Clay in the vicinity of the Liupanshan region and its implications for the early origin of C_4 plants in the Chinese Loess Plateau, *Quat. Sci.,* **31,** 800–811.

Zijderveld, J.D.A., 1967. AC demagnetization of rocks: analysis of results, in *Methods in Paleomagnetism,* pp. 254–286, eds Collinson, D.W., Creer, K.M. & Runcorn, S.K., Elsevier, Amsterdam.